The Astrophysical Journal Letters, 998:L36 (11pp), 2026 February 20 https://doi.org/10.3847/2041-8213/ae382a

ALMA and JWST Identification of Faint Dusty Star-forming Galaxies up to $z \sim 8$ and Their Connection with Other Galaxy Populations

Jorge A. Zavala[1], Andreas L. Faisst[2], Manuel Aravena[3], Caitlin M. Casey[4,5], Jeyhan S. Kartaltepe[6], Felix Martinez, III[6], John D. Silverman[7,8], Sune Toft[5,9], Ezequiel Treister[10], Hollis B. Akins[11], Hiddo Algera[12], Karina Barboza[13,14], Andrew J. Battisti[15,16], Gabriel Brammer[5,9], Zheng Cai[17], Jaclyn Champagne[18], Nicole E. Drakos[19], Eiichi Egami[18], Xiaohui Fan[18], Maximilien Franco[20], Yoshinobu Fudamoto[21], Seiji Fujimoto[22,23], Steven Gillman[5,24], Ghassem Gozaliasl[25,26], Santosh Harish[6], Xiangyu Jin[27], Koki Kakiichi[5,9], Darshan Kakkad[28], Anton M. Koekemoer[29], Ruqiu Lin[1], Daizhong Liu[30], Arianna S. Long[31], Georgios E. Magdis[5,9], Sinclaire Manning[1], Crystal L. Martin[32], Jed McKinney[11], Romain Meyer[33], Giulia Rodighiero[34,35], Victoria Salazar[1], David B. Sanders[36], Marko Shuntov[5,9], Margherita Talia[37,38], Takumi S. Tanaka[7,8,39], Feige Wang[27], Wuji Wang[2], Stephen M. Wilkins[40,41], Jinyi Yang[27], Min S. Yun[1] The CHAMPS and COSMOS-Web collaborations

[1] University of Massachusetts Amherst, 710 North Pleasant Street, Amherst, MA 01003-9305, USA; jzavala@umass.edu
[2] Caltech/IPAC, MS 314-6, 1200 E. California Boulevard, Pasadena, CA 91125, USA
[3] Instituto de Estudios Astrofísicos, Facultad de Ingeniería y Ciencias, Universidad Diego Portales, Av. Ejército 441, Santiago, Chile
[4] Department of Physics, University of California, Santa Barbara, Santa Barbara, CA 93106, USA
[5] Cosmic Dawn Center (DAWN), Denmark
[6] Laboratory for Multiwavelength Astrophysics, School of Physics and Astronomy, Rochester Institute of Technology, 84 Lomb Memorial Drive, Rochester, NY 14623, USA
[7] Kavli Institute for the Physics and Mathematics of the Universe (WPI), The University of Tokyo, Kashiwa, Chiba 277-8583, Japan
[8] Department of Astronomy, School of Science, The University of Tokyo, 7-3-1 Hongo, Bunkyo, Tokyo 113-0033, Japan
[9] Niels Bohr Institute, University of Copenhagen, Jagtvej 128, DK-2200, Copenhagen, Denmark
[10] Instituto de Alta Investigación, Universidad de Tarapacá, Casilla 7D, Arica, Chile
[11] The University of Texas at Austin, 2515 Speedway Boulevard, Stop C1400, Austin, TX 78712, USA
[12] Institute of Astronomy and Astrophysics, Academia Sinica, 11F of Astronomy-Mathematics Building, No. 1, Sec. 4, Roosevelt Road, Taipei 106216, Taiwan, ROC
[13] Department of Astronomy, The Ohio State University, 140 W. 18th Avenue, Columbus, OH 43210, USA
[14] Center for Cosmology and AstroParticle Physics, The Ohio State University, 191 W. Woodruff Avenue, Columbus, OH 43210, USA
[15] International Centre for Radio Astronomy Research, University of Western Australia, 35 Stirling Highway, Crawley, WA 6009, Australia
[16] Research School of Astronomy and Astrophysics, Australian National University, Cotter Road, Weston Creek, ACT 2611, Australia
[17] Department of Astronomy, Tsinghua University, Beijing 100084, People's Republic of China
[18] Steward Observatory, University of Arizona, 933 N. Cherry Avenue, Tucson, AZ 85721, USA
[19] Department of Physics and Astronomy, University of Hawaii, Hilo, 200 W. Kawili Street, Hilo, HI 96720, USA
[20] Université Paris-Saclay, Université Paris Cité, CEA, CNRS, AIM, 91191, Gif-sur-Yvette, France
[21] Center for Frontier Science, Chiba University, 1-33 Yayoi-cho, Inage-ku, Chiba 263-8522, Japan
[22] David A. Dunlap Department of Astronomy and Astrophysics, University of Toronto, 50 St George Street, Toronto, ON M5S 3H4, Canada
[23] Dunlap Institute for Astronomy and Astrophysics, 50 St George Street, Toronto, ON M5S 3H4, Canada
[24] DTU-Space, Technical University of Denmark, Elektrovej 327, DK-2800 Kgs. Lyngby, Denmark
[25] Department of Computer Science, Aalto University, P.O. Box 15400, FI-00076 Espoo, Finland
[26] Department of Physics, University of Helsinki, P.O. Box 64, FI-00014 Helsinki, Finland
[27] Department of Astronomy, University of Michigan, 1085 S. University Avenue, Ann Arbor, MI 48109, USA
[28] Centre for Astrophysics Research, University of Hertfordshire, Hatfield, AL10 9AB, UK
[29] Space Telescope Science Institute, 3700 San Martin Drive, Baltimore, MD 21218, USA
[30] Purple Mountain Observatory, Chinese Academy of Sciences, 10 Yuanhua Road, Nanjing 210023, People's Republic of China
[31] Department of Astronomy, The University of Washington, Seattle, WA 98195, USA
[32] Department of Physics, University of California, Santa Barbara, Santa Barbara, CA 93109, USA
[33] Department of Astronomy, University of Geneva, Chemin Pegasi 51, 1290 Versoix, Switzerland
[34] Dipartimento di Fisica e Astronomia, Università di Padova, Vicolo dell'Osservatorio, 3, I-35122 Padova, Italy
[35] INAF—Osservatorio Astronomico di Padova, Vicolo dell'Osservatorio 5, I-35122 Padova, Italy
[36] Institute for Astronomy, University of Hawai'i at Manoa, 2680 Woodlawn Drive, Honolulu, HI 96822, USA
[37] University of Bologna—Department of Physics and Astronomy "Augusto Righi" (DIFA), Via Gobetti 93/2, I-40129 Bologna, Italy
[38] INAF—Osservatorio di Astrofisica e Scienza dello Spazio, Via Gobetti 93/3, I-40129, Bologna, Italy
[39] Center for Data-Driven Discovery, Kavli IPMU (WPI), UTIAS, The University of Tokyo, Kashiwa, Chiba 277-8583, Japan
[40] Astronomy Centre, University of Sussex, Falmer, Brighton BN1 9QH, UK
[41] Institute of Space Sciences and Astronomy, University of Malta, Msida MSD 2080, Malta
Received 2025 September 25; revised 2026 January 12; accepted 2026 January 13; published 2026 February 11

Abstract

We exploit a new sample of around 400 bright dusty galaxies from the Atacama Large Millimeter/submillimeter Array (ALMA) CHAMPS Large Program, together with the rich JWST multiband data products in the COSMOS field, to explore and validate new selection methods for identifying dusty star-forming galaxies (DSFGs).

Here we present an effective empirical selection criterion based on a newly defined parameter: $I_\star \equiv \log_{10}(M_\star) \times \log_{10}(\mathrm{SFR})$. Incorporating the $m_{277\mathrm{W}} - m_{444\mathrm{W}}$ color as a second parameter further improves the purity of the selection. We then apply this method to the COSMOS2025 catalog to search for fainter dusty galaxy candidates below the ALMA CHAMPS detection limit and, through a stacking technique, identify a population of high-redshift DSFG candidates with an average flux density of $S_{1.2\mathrm{mm}} \approx 150\,\mu$Jy and a space density of $\sim 6 \times 10^{-6}\,\mathrm{Mpc}^{-3}$. Three of these galaxies have been spectroscopically confirmed at $z_{\mathrm{spec}} = 7.20$, 5.85, and 5.04. This faint population seems to have been missed by most of the previous submillimeter/millimeter surveys and ground- and space-based UV−near-IR observations. We then show evidence of a possible evolutionary connection between the $z > 10$ UV-bright galaxies recently discovered by JWST, the faint dusty $z \approx$ 6-8 galaxies identified here, and the population of $z \approx$ 3–5 massive quiescent galaxies; all of them are potentially linked as progenitor−descendant populations based on their abundance, redshifts, and stellar masses. Future spectroscopic campaigns will be essential to confirm the redshifts and physical properties of these massive, faint, high-redshift DSFG candidates.

Unified Astronomy Thesaurus concepts: Galaxies (573); High-redshift galaxies (734); Dust continuum emission (412); Star formation (1569); Early universe (435); Galaxy evolution (594); Submillimeter astronomy (1647); Millimeter astronomy (1061); James Webb Space Telescope (2291)

1. Introduction

Submillimeter-selected galaxies (broadly called dusty star-forming galaxies (DSFGs); see reviews by C. M. Casey et al. 2014; J. A. Hodge & E. da Cunha 2020) are among the most extreme dust-enshrouded extragalactic systems. They have been shown to account for the majority of massive ($M_\star \gtrsim 10^{10}\,M_\odot$) star-forming galaxies at redshifts of $z \approx$ 2–4 (e.g., J. S. Dunlop et al. 2017; T. Wang et al. 2019; U. Dudzevičiūtė et al. 2020; A. S. Long et al. 2023; F.-Y. Liu et al. 2026) and to contribute significantly to the cosmic star formation history (e.g., J. A. Zavala et al. 2021). However, their physical properties and abundance, particularly at $z > 6$, remain highly uncertain (e.g., H. S. B. Algera et al. 2023). This represents an important gap in our current census of galaxies and in our understanding of the earliest phases of galaxy formation.

This challenge is twofold. First, the apparent rarity of DSFGs at high redshifts (compared to their lower-redshift counterparts) requires relatively deep and wide-area (sub) millimeter surveys to directly identify them via their dust continuum emission. Such surveys remain scarce and expensive with current instrumentation, and as a result, existing samples of DSFGs (or candidates) at $z > 6$ are very limited. Second, because of their high dust obscuration, these systems are typically faint at rest-frame UV/optical wavelengths, with many of them undetected even in the deepest Hubble Space Telescope (HST) images (e.g., D. H. Hughes et al. 1998; E. Daddi et al. 2009; M. Franco et al. 2018; Y. Fudamoto et al. 2021; S. M. Manning et al. 2022; I. Smail et al. 2023)—a problem that becomes increasingly severe at higher redshifts owing to the strong *K*-correction in these wave bands. This has historically hindered their identification, confirmation, and characterization. However, this is set to change soon.

The high sensitivity and long-wavelength coverage of the instruments on board JWST promise to provide the long-needed data to study the stellar light of these galaxies. In fact, there are a growing number of DSFGs observed with JWST observations, and most of them are clearly detected by the NIRCam camera (particularly in the reddest filters; e.g., C.-C. Chen et al. 2022; T. Herard-Demanche et al. 2025; J. A. Hodge et al. 2025; S. M. Manning et al. 2025; J. McKinney et al. 2025; H. Umehata et al. 2026; but see F. Sun et al. 2025 for a counterexample). This can be exploited not only to characterize current samples of dusty galaxies but also to develop new selection methods to identify new dusty candidates. This, combined with the new generation of submillimeter/millimeter surveys, promises to complete our census of dust-obscured star formation during the Universe's first Gyr.

In this work, we take advantage of a new large sample of around 400 bright millimeter-selected sources to test the use of JWST observations (and associated catalogs) for identifying DSFG candidates at $z > 6$. These 400 objects were selected from the COSMOS High-z ALMA-MIRI Population Survey (CHAMPS) Atacama Large Millimeter/submillimeter Array (ALMA) Large Program (proposal No. 2023.1.00180.L; A. Faisst et al. 2026, in preparation; F. Martinez et al. 2026, in preparation). Our goals are (1) to provide and validate efficient JWST selection diagrams for DSFGs and (2) to use these diagrams to search for a population of faint, high-redshift dusty systems to constrain the prevalence of DSFGs in the early Universe. The physical characterization of the CHAMPS galaxies is not part of this work and will be presented in a forthcoming work.

This Letter is structured as follows: Section 2 presents the ALMA and JWST datasets used in this study. The proposed selection diagrams for identifying DSFGs are presented in Section 3, and their application to search for $z \approx$ 6–8 systems is presented in Section 4. The 18 dusty candidates found within this redshift range are also presented in Section 4, along with a discussion of their properties in the context of other galaxy populations. Finally, we summarize our results in Section 5. Throughout this Letter, we adopt a ΛCDM cosmology with $\Omega_m = 0.32$, $\Omega_\Lambda = 0.68$, and $h = 0.696$.

2. Sample Selection and Observations

2.1. The ALMA CHAMPS Galaxy Sample

CHAMPS is a Cycle 10 ALMA Large Program covering a total area of 0.18 deg^2 with continuum observations at 1.2 mm (≈243 GHz). The observations have an average 1σ rms sensitivity of $1\sigma_{1.2\mathrm{mm}} \approx 120\,\mu$Jy and an average angular resolution of $\theta_{\mathrm{FWHM}} \approx 1''$. The mosaic layout, which covers a total area of ≈0.18 deg^2, was designed to overlap with the MIRI imaging of the JWST COSMOS-Web survey (C. M. Casey et al. 2023; S. Harish et al. 2025) and consists of 43 independent mosaics (or *boxes*) that were observed separately and processed independently. The imaging of the

uv-visibilities was done using CASA, with a natural weighting approach to maximize the sensitivity. Further details of the program, observing setup, and data reduction will be presented in F. Martinez et al. (2026, in preparation).

We build our galaxy sample through a simple peak-search detection algorithm (e.g., J. S. Dunlop et al. 2017) with a conservative selection threshold of 5σ. During this process, the noise in each ALMA mosaic was adopted to be the 68th percentile of the pixel values within the corresponding *box* (equivalent to one standard deviation in the case of a Gaussian distribution) after applying a 5σ clipping to remove the bright sources.

Following this methodology, we identify a sample of around 420 candidates at $>5\sigma$ in the CHAMPS survey, with a typical flux density range of $S_{1.2\mathrm{mm}} \approx 0.6$–$2.0$ mJy. Note that the final CHAMPS catalog, which explores multiple selection techniques and signal-to-noise ratio (SNR) thresholds, will be presented in F. Martinez et al. (2026, in preparation), along with the completeness and the expected false detection rate, but we highlight that the contamination fraction of our sample is below 5% (based on the ratio of negative to positive pixels in the map).

Here we use this conservative sample to construct a new selection diagram for DSFGs based purely on JWST observations, as described in the next sections.

2.2. Identification of JWST Counterparts

To identify JWST counterparts for our ALMA-selected galaxies, we make use of the COSMOS2025 catalog (M. Shuntov et al. 2025). This catalog is based on the JWST observations of the COSMOS-Web survey (C. M. Casey et al. 2023), which provides deep imaging in four NIRCam filters (F115W, F150W, F277W, F444W; M. Franco et al. 2025) plus parallel MIRI observations in one filter (F770W; S. Harish et al. 2025). The catalog also includes additional photometric constraints based on several ground- and space-based data, including up to 37 bands spanning 0.3–8 μm. Note that the adopted CHAMPS mosaic layout ensures the availability of both NIRCam and MIRI photometry for our galaxies, which increases the robustness of the spectral energy distribution (SED) fitting results.

During the counterpart matching, we use only galaxies in the COSMOS2025 catalog with quality flags[42] `warn_flag=0` and `warn_flag=2` and a search radius of $0\farcs75$ centered at the ALMA positions (comparable to the measured rest-frame optical size for other DSFGs; S. Gillman et al. 2023), although we note that the vast majority ($\sim$94%) of the matches lie within a $0\farcs3$ radius.

After this process, we identify 378 CHAMPS galaxies with matches in the COSMOS2025 catalog. The remaining $\sim$10% without matches can be explained by different reasons, including a larger positional uncertainty (due to low SNR or blending of close sources), contamination from false detections, sources close to JWST artifacts and/or masked areas, objects with additional flags in the COSMOS2025 catalog, or real sources undetected by JWST. These sources, whose nature and demographics will be presented in a future study, are not included in this work. We note, however, that since our goal is to perform a population-level characterization, excluding these missing sources has a negligible impact on the conclusions drawn from this work.

Hereafter we will focus on this subsample of 378 galaxies with both ALMA and JWST constraints. Across this work, when using the SED-based properties of the COSMOS2025 catalog, we adopt the LePHARE results and the model photometry (M. Shuntov et al. 2025).

3. New DSFG Selection Diagrams

Armed with a large sample of DSFGs and the rich information from the COSMOS2025 catalog that includes not only JWST photometry in several filters but also galaxies' physical properties inferred from multiwavelength SED modeling, here we explore different diagrams and multidimensional spaces to efficiently isolate and distinguish DSFGs from other populations.

3.1. Color–Color and Color–Magnitude Selection Diagrams

We start by exploring several color–magnitude and color–color diagrams to isolate DSFGs. In this comparison, we also include other objects known to have red optical/near-infrared colors, namely $z > 2$ massive quiescent galaxies and the JWST-discovered population of little red dots (LRDs; e.g., G. Barro et al. 2024; J. E. Greene et al. 2024; J. Matthee et al. 2024). We use only samples within the COSMOS-Web field to ensure a homogeneous photometry. For the quiescent systems we use the samples from W. M. Baker et al. (2026) and A. Long et al. (2026, in preparation), and we use the sample of H. B. Akins et al. (2024) for the LRDs.

Figure 1 shows two diagrams that seem useful to separate these populations of galaxies, one based only on NIRCam photometry and the second combining NIRCam and MIRI measurements. As can be seen in the first panel, the majority of ALMA/CHAMPS galaxies have $m_{277\mathrm{W}}$–$m_{444\mathrm{W}} \approx 0.6$–$2.0$ and a redshift-dependent $m_{277\mathrm{W}}$ magnitude as faint as $\approx$26–27. The massive quiescent galaxies show less red colors ($m_{277\mathrm{W}}$–$m_{444\mathrm{W}} \approx 0.0$–$0.6$), while LRDs occupy a locus defined by $m_{277\mathrm{W}}$–$m_{444\mathrm{W}} \approx 1.2$–$3.0$ and $m_{277\mathrm{W}} \approx 25$–$29$ (without mentioning their characteristic point-like morphology). In the right panel, we can see a clear redshift trend in the $m_{444\mathrm{W}}$–$m_{770\mathrm{W}}$ color for the CHAMPS galaxies (a similar trend also exists for $m_{277\mathrm{W}}$–$m_{444\mathrm{W}}$, but with slightly larger scatter). Notably, both LRDs and massive quiescent galaxies are, on average, fainter in the MIRI F770W filter compared to the DSFGs, resulting in less red $m_{444\mathrm{W}}$–$m_{770\mathrm{W}}$ colors (typically associated with a lack of hot dust emission).

While these diagrams are definitely useful to separate DSFGs from the bulk population of galaxies, they are not free of contamination from other systems. For this reason, and because similar color–color and color–magnitude plots have already been discussed in the literature (although with smaller samples of galaxies; e.g., A. J. Barger & L. L. Cowie 2023; P. G. Pérez-González et al. 2023; L. Barrufet et al. 2023; C. C. Williams et al. 2024; J. McKinney et al. 2025; S. J. McKay et al. 2025), below we explore new selection diagrams based on physical properties inferred from SED modeling (e.g., C. Conroy 2013). This is now possible thanks to the rich ancillary data available in some of the extragalactic fields and the unparalleled public data products, such as the COSMOS2025 catalog.

[42] Galaxies with `warn_flag=0` correspond to the most secure sources in the catalog, while sources with `warn_flag=2` are sources with highly uncertain or unreliable ground-based photometry but with reliable space-based measurements (see details in M. Shuntov et al. 2025).

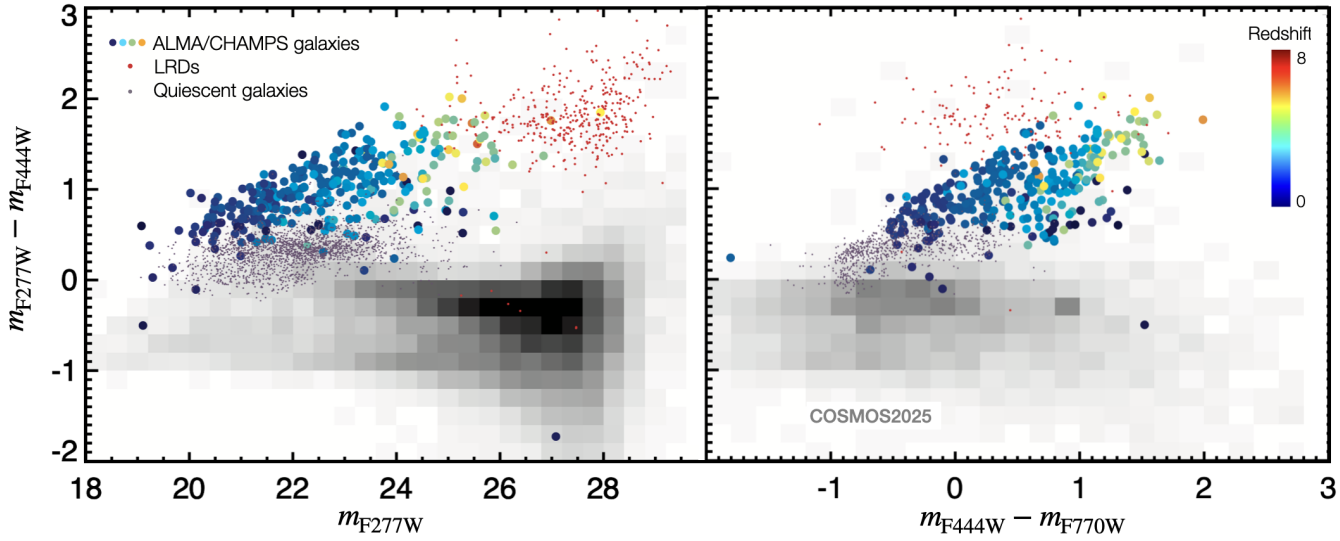

Figure 1. The distribution of galaxies in the COSMOS2025 catalog on the $m_{\rm F277W}$ vs. $m_{277\rm W} - m_{444\rm W}$ (left) and $m_{444\rm W} - m_{770\rm W}$ vs. $m_{277\rm W} - m_{444\rm W}$ (right) planes is illustrated with the gray scale (the darker the color, the higher the number of galaxies). The lighter-gray tones in the right panel are the result of the significantly lower number of galaxies detected with MIRI with respect to the NIRCam-detected objects. Galaxies detected at $>5\sigma$ in the CHAMPS survey are represented by the large circles and color-coded according to their COSMOS2025 photometric redshifts. Massive, $z > 2$ quiescent galaxies (W. M. Baker et al. 2026; A. Long et al. 2026, in preparation) and LRDs (H. B. Akins et al. 2024) are shown as purple and red circles, respectively.

3.2. SED-based Selection Diagrams

It is well established that stellar mass correlates strongly with dust-obscured star formation rate (SFR; e.g., J. S. Dunlop et al. 2017; K. E. Whitaker et al. 2017), making $M_\star$ a potentially effective criterion for identifying DSFGs. However, at lower redshifts, quiescent galaxies dominate the high-mass end of the population and could introduce significant contamination. To mitigate this limitation, in this study we explore alternative selection criteria, including simple SFR cuts and combined criteria based on both SFR and $M_\star$.

As discussed more deeply in Appendix C, a simple SFR cut does a good job of isolating the CHAMPS-detected galaxies from the bulk of galaxies in the COSMOS2025 catalog. We found, however, that a parameter involving both SFR and $M_\star$ performs even better.

Here we introduce the *stellar index*, or simply $I_\star$, defined as

$$I_\star \equiv \log_{10}(M_\star/M_\odot) \times \log_{10}(\mathrm{SFR}/M_\odot\ \mathrm{yr}^{-1}). \quad (1)$$

We estimate this parameter for all the galaxies in the COSMOS2025 catalog, including our ALMA/CHAMPS sources, and the quiescent galaxies and LRDs mentioned above, using the stellar masses and the SFRs from the LePhare SED fitting results reported in the catalog. While this construction, coupling the stellar mass and SFR in logarithmic space, is unusual and lacks a direct physical interpretation, it provides a useful diagnostic for distinguishing galaxy populations—particularly at the high-mass end—with a transition from positive to negative values at SFR $= 1\,M_\odot\,\mathrm{yr}^{-1}$ (see Appendix B for a deeper discussion of this parameter).

The left panel of Figure 2 shows all these galaxies on the plane formed by $I_\star$ and the NIRCam-based $m_{277\rm W} - m_{444\rm W}$ color. As can be seen, the majority of the ALMA/CHAMPS galaxies occupy a unique locus on this plane, with high $I_\star \gtrsim 15$ values and red colors ($m_{277\rm W} - m_{444\rm W} \gtrsim 0.5$), by virtue of their high stellar masses and SFRs and their high dust attenuation (see Appendix C for a comparison with other similar diagrams). On the contrary, the majority of the JWST-selected galaxies have $I_\star \sim 0$ and $m_{277\rm W} - m_{444\rm W} \sim 0$ and skew toward negative $I_\star$ values and bluer colors.

Compared to the color–color and color–magnitude plots discussed above, this diagram does a better job at separating the massive quiescent galaxies from the DSFG population, with the former having very low $I_\star$ values owing to their low SFR (and having red colors owing to their old stellar populations).

The positions of the LRDs in this plot, with comparable $I_\star$ as some of the DSFGs, might seem surprising. Nevertheless, it is well-known that, when a pure galaxy SED model is adopted, inferences based on SED fitting techniques lead to very large stellar masses (and thus high $I_\star$ values; e.g., I. Labbé et al. 2023; H. B. Akins et al. 2024). However, recent results suggest that LRDs are likely dominated by AGN activity and, thus, the stellar masses and SFRs reported in the COSMOS2025 catalog (and adopted in this work) are most likely incorrect (see B. Wang et al. 2024 for a thorough discussion of the typical uncertainties of these parameters). These SED-based results—which are not used anywhere else in the Letter—are, however, useful to isolate them in this diagram.

The right panel of Figure 2 shows, again, the product between the logarithm of the stellar mass and the logarithm of the SFR for galaxies in the COSMOS2025 catalog, but now as a function of the COSMOS2025 photometric redshift and color-coded by their mean $m_{277\rm W} - m_{444\rm W}$ color. This figure reveals that galaxies with $I_\star \gtrsim 20$ have systematically red colors virtually from $z \approx 0$ to $z \approx 10$ and thus should be dominated by DSFGs and/or LRDs. Note that sources with such high $I_\star$ values are very rare in the catalog, as indicated by the contours in the figure.

This figure also reveals a few other interesting points. First, we can see at $z \sim 5.7$ and $z \sim 7.9$ an excess of red sources with respect to the average trend. At these redshifts, the Hα and

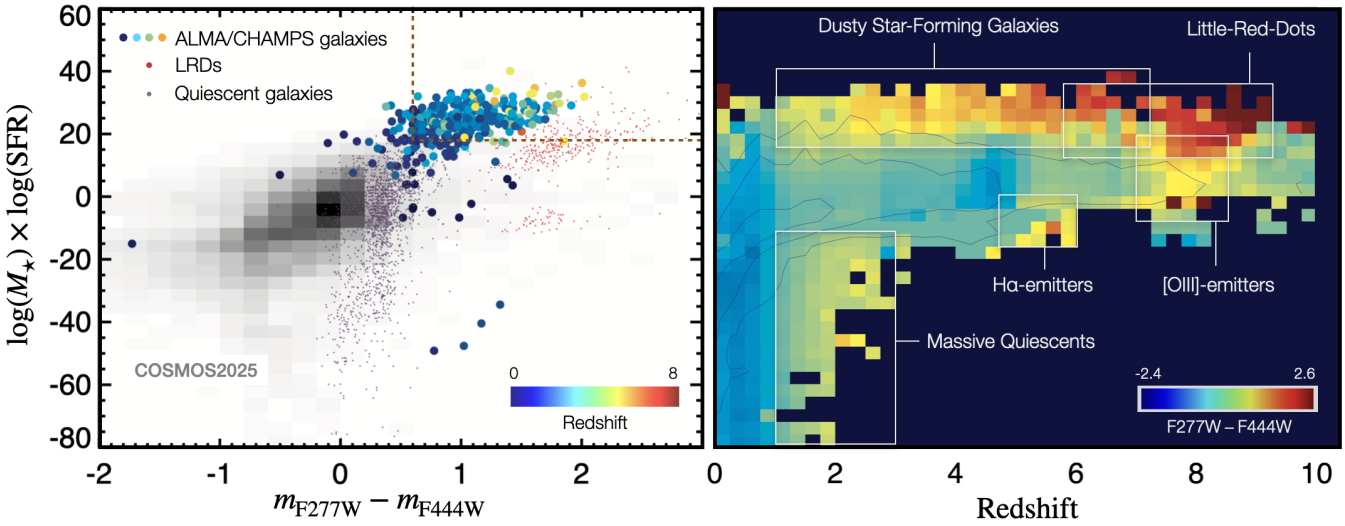

Figure 2. Left: analog to Figure 1, but for the $m_{277\mathrm{W}} - m_{444\mathrm{W}}$ vs. $I_\star$ plane. The red dotted lines delineate the locus preferentially occupied by DSFGs, which is also used in Section 4 to select high-redshift dusty candidates (note that LRDs are excluded from this selection by imposing a size cut). Right: the COSMOS2025 galaxies in the $I_\star$–z plane, with contours indicating the source density in steps of 1 dex. Each grid cell is colored according to the corresponding galaxies' mean $m_{277\mathrm{W}} - m_{444\mathrm{W}}$ color. Galaxies with high $I_\star$ values of $\gtrsim$15 have systematically redder colors than those from the bulk population. Other populations of red $m_{277\mathrm{W}} - m_{444\mathrm{W}}$ sources, but with lower $I_\star$—including quiescent galaxies and line emitters at specific redshifts—are also highlighted.

[O III] lines fall within the F444W filter. We therefore suggest that these two populations likely correspond to Hα and [O III] emitters, with emission lines contaminating the F444W photometry. Similarly, sources with blue $m_{277\mathrm{W}} - m_{444\mathrm{W}}$ colors at $z \sim 4.5$ could correspond to [O III] emitters, with their emission lines boosting the F277W photometry. Finally, it can also be seen that the population of massive quiescent galaxies, with red colors and low $I_\star$, statistically appears at $z \sim 3$ and dominates this parameter space within $z \approx$ 1–3. At lower redshift, galaxies with low $I_\star$ are mostly low-mass galaxies with blue colors.

The product between the logarithm of the stellar mass and the logarithm of the SFR, $I_\star$, in combination with other parameters like the $m_{277\mathrm{W}} - m_{444\mathrm{W}}$ color and redshift, seems thus to be a powerful way of discriminating (and selecting) different populations of galaxies, and it is potentially useful to identify dusty star-forming galaxies, as discussed in the next sections.

4. On the Search for High-redshift Dusty Galaxies

Despite the successful detection of dust continuum emission in a few tens of spectroscopically confirmed galaxies at $z > 6$ (e.g., D. Watson et al. 2015; T. Hashimoto et al. 2019; T. J. L. C. Bakx et al. 2021; N. Laporte et al. 2021; H. Inami et al. 2022; S. Schouws et al. 2022; R. Endsley et al. 2023; M. Castellano et al. 2025; F. Sun et al. 2025), the volume density of such high-redshift dusty systems, as well as their contribution to the cosmic star formation history, remains highly uncertain. This issue is closely tied to the small sample sizes of these studies—often limited to only one or two sources—as well as to the challenges inherent in their identification methods. Such methods include, for example, searches sensitive only to extreme starburst or gravitationally amplified systems (e.g., D. P. Marrone et al. 2018; J. A. Zavala et al. 2018; S. Fujimoto et al. 2021) or serendipitous detections around quasar and/or other massive galaxies (e.g., R. Decarli et al. 2017; Y. Fudamoto et al. 2021; F. Sun et al. 2025).

Here, taking advantage of the well-defined and relatively large area of the ALMA CHAMPS 1.2 mm imaging—which also benefits from NIRCam and MIRI imaging and the rich legacy of the COSMOS2025 catalog—we attempt to identify high-redshift ($z \approx$ 6–8) DSFGs and to put constraints on their number density and millimeter brightness through a stacking analysis.

4.1. Selection of Faint DSFG Candidates

Based on the results from Section 3, first we identify dusty star-forming galaxy candidates by selecting all the sources in the COSMOS2025 catalog that satisfy the following criteria (see also Figure 2):

$$\begin{cases} I_\star > 17, \\ m_{\mathrm{F277W}} - m_{\mathrm{F444W}} > 0.6, \quad \text{and} \\ 6 < z_{\mathrm{phot}} < 8. \end{cases}$$

Then, we remove all point-like sources by comparing the aperture photometry measured within 0.″2 and 0.″5. Following H. B. Akins et al. (2024), we remove all objects with $S_{\mathrm{F444W}}(0.''2)/S_{\mathrm{F444W}}(0.''5) > 0.5$ (this is actually the inverse of the H. B. Akins et al. 2024 selection criterion since they were interested in selecting compact objects and LRD candidates). Note that this cut also removes imaging artifacts with apparent sizes smaller than the PSF. This results in a selection of only 73 galaxies, which illustrates the rareness of this kind of object, representing only ∼0.01% of the whole catalog (and ∼1% of the sources within $6 \leqslant z_{\mathrm{phot}} \leqslant 8$).

However, not all of these 73 galaxies are covered by the CHAMPS survey since the CHAMPS area of 0.18 deg^2 (driven by the available MIRI imaging at the time of the survey design) represents only ∼30% of the whole COSMOS-Web NIRCam imaging, the base of the COSMOS2025 catalog.

Figure 3. The top right panel shows the stacking of the CHAMPS 1.2 mm data at the position of the 18 $z \approx 6$–8 DSFG candidates identified in Section 4 (and shown on the left, with their respective COSMOS2025 IDs). The 5σ detection in the stack implies an average flux density of $S_{1.2\mathrm{mm}} = 0.16 \pm 0.03$ mJy, confirming both the effectiveness of our selection method to identify dusty candidates and the existence of a dust-enshrouded population of galaxies within the epoch of reionization. The bottom right panel shows the results of a similar stacking procedure but centered at the position of random sources from the COSMOS2025 catalog, which results in a nondetection.

From these 73 objects, there are only 20 galaxies within the CHAMPS coverage that can be used for the stacking analysis. We visually inspect all of them and finally remove two objects, one potential image artifact and an object on top of a diffraction spike (IDs: 89430 and 703091). The remaining sources (shown in Figure 3) are adopted as our final sample of $z \approx 6$–8 DSFG candidates and used below in a stacking analysis to put constraints on their dust continuum emission. All of them have best-fit stellar masses of $M_\star > 10^{10}\,M_\odot$ in the COSMOS2025 catalog, with the exception of two systems, and SFRs above $50\,M_\odot\,\mathrm{yr}^{-1}$.

We finally confirm that none of these 18 galaxies are detected in the CHAMPS mosaic (all being below the 3σ level) and that they have not been reported in previous (sub) millimeter catalogs such as SCUBADive (J. McKinney et al. 2025), exMORA (A. S. Long et al. 2024), or A3COSMOS (D. Liu et al. 2019; F.-Y. Liu et al. 2026).

4.2. Stacking Analysis

Here we stack the ALMA CHAMPS data (in the image plane) at the position of the 18 high-redshift DSFG candidates reported above. For this purpose, we use an inverse-variance-weighted mean defined as $\widehat{\mu} = \sum_{i=1}^{n}(x_i \cdot w_i)/\sum_{i=1}^{n} w_i$, where the weights, w_i, are given by $1/\sigma_i^2$, with σ_i being the standard deviation of the pixel values in each cutout image. The stack results in a $\sim 5.0\sigma$ detection of dust continuum emission (see Figure 3) with a peak flux density of $S_{1.2\mathrm{mm}} = 0.16 \pm 0.03$ mJy, with the error estimated as $\sigma_{\widehat{\mu}} = \sqrt{1/\sum_i w_i}$. Assuming a typical modified blackbody for the dust SED ($T_D \approx 35\,K$, $\beta \approx 2$; e.g., C. M. Casey 2012) and an $L_{\mathrm{IR}(8-1000\mu\mathrm{m})}$–SFR conversion factor (R. C. Kennicutt & N. J. Evans 2012), the inferred 1.2 mm flux density would translate into a dust-obscured star formation of $\sim 30\,M_\odot\,\mathrm{yr}^{-1}$.

A potential drawback of this method, though, is that it is prone to statistical outliers, without mentioning the fact that the estimated error depends only on the data uncertainties but not on the data spread. To take this into account, we quantify the uncertainties through a bootstrapping technique, randomly drawing 15 objects at a time (allowing a single object to appear more than once) before estimating the weighted mean as described above. After 100 iterations, we measure the average and standard deviation of the weighted mean to be $S_{1.2\ \mathrm{mm}} = 0.15 \pm 0.02$ mJy, in good agreement with the value reported above.

To further test the significance of the detection, we repeat the exact same procedure but now stacking the CHAMPS data at random positions and at the position of randomly selected sources from the COSMOS20205 catalog (keeping the same number of sources as in our main stacking). These tests result in nondetections, as illustrated by an example included in Figure 3.

Two conclusions can be drawn from these results. First, this demonstrates the effectiveness of the proposed selection method (based on $I_\star$ and the $m_{277\mathrm{W}} - m_{444\mathrm{W}}$ color) to identify DSFG candidates, and second, it confirms the existence of a high-redshift population of faint dusty galaxies that contribute to the cosmic history of star formation, even up to $z \sim 8$ (see also H. S. B. Algera et al. 2023; L. Barrufet et al. 2023; G. Rodighiero et al. 2023; S. Fujimoto et al. 2024; C. C. Williams et al. 2024; M. Xiao et al. 2024; L. Bing et al. 2025).

It is worth noting that most of these galaxies are undetected or very faint in the bluest NIRCam filters of COSMOS-Web and in most of the available data at $\lambda_{\mathrm{obs}} \lesssim 1.15\,\mu$m, meaning that they were missed in pre-JWST studies. As a reference, six of these galaxies are undetected in the F115W filter, and the median magnitude of those detected is $m_{\mathrm{F115W}} \approx 27$. Additionally, seven are undetected or fainter than 27 mag in F150W, which is similar to the typical 5σ detection limit of HST/F160W surveys. Similarly, because of their faintness at millimeter wavelengths—being around one order of magnitude fainter than the CHAMPS-detected sources—these high-redshift DSFGs would remain undetected in most of the submillimeter/millimeter surveys available to date.

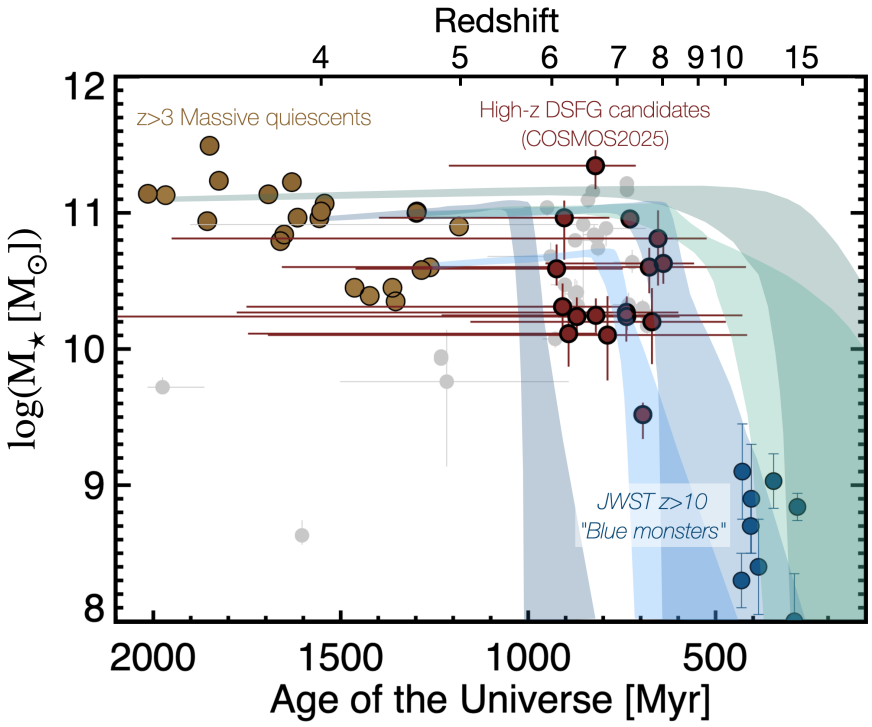

Figure 4. Stellar masses as a function of redshift for different populations of galaxies, including spectroscopically confirmed massive quiescent galaxies at $z > 3$ (gold circles; A. C. Carnall et al. 2024; K. Glazebrook et al. 2024; A. de Graaff et al. 2025; K. Ito et al. 2025), JWST-selected galaxies at $z > 10$ (blue circles; P. Arrabal Haro et al. 2023; A. J. Bunker et al. 2023; S. Carniani et al. 2024; M. Castellano et al. 2024; R. P. Naidu et al. 2025; J. A. Zavala et al. 2025), and our $z \approx 6$–8 DSFG candidates (red and gray circles). The gray circles represent the best-fit parameters obtained when including the submillimeter photometry in the SED fitting (see Section 4.3). We also include the evolutionary track of the five massive galaxies from A. C. Carnall et al. (2024; blue/green shaded areas), which nicely connect the three different populations. This supports a potential evolutionary link between the $z > 10$ galaxies recently discovered with JWST, $z \gtrsim 6$ DSFGs, and $z \approx 3$–5 massive quiescent galaxies, all of them having a comparable comoving volume density (see Section 4.3).

Finally, we point out that the inferred average IR-based SFR of these galaxies of $30\,M_{\odot}\,\mathrm{yr}^{-1}$ is comparable to or smaller than the dust-corrected SFR from the COSMOS2025 catalog. In fact, the median $\mathrm{SFR_{IR}}/\mathrm{SFR_{LePHARE}}$ ratio is approximately 0.25, indicating that dust-obscured star formation in these faint systems is not the dominant component. This population may therefore bridge the gap between dust-free UV-bright galaxies and more massive dusty systems, providing insights into dust formation processes at high redshift (e.g., T. J. L. C. Bakx et al. 2025; I. Mitsuhashi et al. 2025).

4.3. Constraining Their Volume Density and Potential Evolution

Based on the 18 candidates reported above and the 0.18 deg^2 area blindly covered by the CHAMPS survey, we estimate a surface density of $0.027^{+0.008}_{-0.006}$ arcmin^{-2} and, considering the redshift range of $z = 6$–8, a comoving volume density of $5.9^{+1.8}_{-1.3} \times 10^{-6}\,\mathrm{Mpc}^{-3}$ (where the error bars represent the 84% Poisson confidence interval; N. Gehrels 1986). The cosmic sample variance uncertainty within this redshift range is expected to be around 13% (according to the formalism derived by S. P. Driver & A. S. G. Robotham 2010 and implemented by the ICRAR cosmology calculator),[43] which is relatively small compared to other surveys covering smaller areas.

The inferred space density for these objects is comparable to the abundance of bright ($M_{\mathrm{UV}} \lesssim -20.5$) galaxies at $z \approx 11$–14, constrained to be from a few times $10^{-6}\,\mathrm{Mpc}^{-3}$ to a few times $10^{-5}\,\mathrm{Mpc}^{-3}$ (e.g., M. Castellano et al. 2023; C. M. Casey et al. 2024; C. T. Donnan et al. 2024; S. L. Finkelstein et al. 2024; M. Franco et al. 2024; Y. Asada et al. 2026; Y. Harikane et al. 2025), although leaning toward the lowest estimations. Note, however, that the inferred space density reported above for DSFGs does not include brighter sources that would be detected above 5σ in the CHAMPS catalog (like those systems recently reported by R. Endsley et al. 2023; M. Xiao et al. 2024; F. Sun et al. 2025). Including those objects would increase the comoving volume density by up to a factor of 2×, making the agreement with some of the reported $z > 10$ galaxies' source density even better.

The comoving volume density of these two populations is also similar to that of the massive ($\log(M_{\star}/M_{\odot}) \gtrsim 10.5$) quiescent galaxies at $z \approx 3$–5, constrained to be around $2 \times 10^{-5}\,\mathrm{Mpc}^{-3}$ (with field-to-field variations of the order of 2–3×; e.g., F. Valentino et al. 2023). This can be interpreted as evidence for a potential progenitor–descendant link between these populations as further explored below (see also F. Sun et al. 2025).

To further test this scenario, in Figure 4 we compare the stellar masses and redshifts of these three populations with the predicted stellar mass growth of quiescent systems according to available constraints on their star formation histories. The stellar masses and redshifts of the quiescent galaxies and $z > 10$ galaxies are taken from the literature (see figure caption for details), whereas the properties of the high-redshift dusty candidates identified in this work are taken from the COSMOS2025 catalog. As can be seen, the stellar masses of the $z \approx 6$–8 DSFG candidates (which

[43] https://cosmocalc.icrar.org

range from $\sim 10^{10}$ to $\sim 10^{11}\,M_{\odot}$) and those from the $z > 10$ sources ($\approx 10^{8}$–$10^{9}\,M_{\odot}$) are in good agreement with the expected evolutionary track of the $z > 3$ massive quiescent galaxies. In other words, the high-z DSFG candidates reported here are consistent with being the progenitors of massive quiescent galaxies and the descendants of the $z > 10$ bright systems. This scenario is supported not only by their inferred redshifts and masses but also by their similar comoving volume densities, as described above (see also F. Sun et al. 2025), although we acknowledge that this might not be the only evolutionary pathway for all these systems.

4.4. Caveats and Limitations of Redshift Estimates

Without spectroscopic confirmation, the redshifts of our dusty candidates—and thus their inferred physical properties—are very uncertain (see uncertainties in Figure 4). A few of them have indeed secondary redshift solutions at $z \sim 3$–5, a well-known problem for dusty systems (e.g., J. A. Zavala et al. 2023; S. Jin et al. 2024; A. J. Battisti et al. 2025).

To test the reliability of the adopted photometric redshifts and to minimize potential biases related to the adopted SED fitting code, we refit the JWST photometry of our high-redshift DSFG candidates using a different software (i.e., BAGPIPES; A. C. Carnall et al. 2018) and including the average 1.2 mm flux density derived from the stacking procedure, which can break the well-known dust/age degeneracy. Each galaxy was fitted twice, first using aperture photometry and then using the model-based photometry (see M. Shuntov et al. 2025 for details). We remind the reader that all of these galaxies benefit from MIRI coverage per design, which typically improves the SED fitting results (e.g., C. Papovich et al. 2023; T. Wang et al. 2025). Reassuringly, this independent fitting procedure confirms that the majority of these sources lie within $z \approx 6$–8, with only $\lesssim$20% of them having best-fit photometric redshifts of $z \lesssim 6$ (see gray circles in Figure 4). We stress, however, that both spectroscopic redshift confirmation and direct submillimeter/millimeter detection are necessary to further test the proposed scenario and to constrain the nature of these objects.

With this in mind, we exploit the available spectroscopic data from the JWST/COSMOS-3D program (GO#5893; K. Kakiichi et al. 2024) and search for any detections in these galaxies, finding robust detections in two galaxies and tentative lines in three other objects. We include the spectra of the two robust detections (IDs 386433 and 469510) in Appendix A. The former shows three emission lines that correspond to the [O III] doublet and $H\beta$, which implies a spectroscopic redshift of $z_{\rm spec} = 7.20$. In fact, this object was included in the recent study of [O III] line emitters presented by R. A. Meyer et al. (2025). The latter shows a single line that is likely associated with Hα at $z_{\rm spec} = 5.04$ (or, alternatively, [O III] at 6.86). We finally noticed that one of our tentative detections (ID = 662086) was indeed confirmed by H. B. Akins et al. (2025) to lie at[44] $z_{\rm spec} = 5.836$ based on the JWST/NIRSpec observations of the CAPERS program (GO#6368; P.I. M. Dickinson; C. T. Donnan et al. 2025; A. J. Taylor et al. 2025).

Although these spectra confirm the high-redshift ($z > 5$) nature of these galaxies, two of them fall below our photometric redshift threshold of $z \sim 6$. This strengths the importance of confirming the redshifts and physical properties of these galaxies. Upcoming spectroscopic campaigns using the NIRSpec multiobject spectroscopy mode (similar to the CAPERS survey; M. Dickinson et al. 2024) and the NIRCam Wide Field Slitless Spectroscopy mode (such as FRESCO and COSMOS-3D; P. A. Oesch et al. 2023; K. Kakiichi et al. 2024) will be critical in this effort.

[44] This source is part of the galaxy overdensity reported by H. B. Akins et al. (2025) around MAMBO-9, a brighter DSFG at $z = 5.85$.

5. Summary

1. Using the combination of the ALMA CHAMPS Large Program and the JWST-based COSMOS2025 catalog in the COSMOS-Web field, we showed that DSFGs have unique properties compared to the bulk population of galaxies detected with JWST. The ALMA-detected galaxies have among the largest stellar masses ($M_{\star} \gtrsim 10^{10}\,M_{\odot}$) and SFRs ($\gtrsim 100\,M_{\odot}\,{\rm yr}^{-1}$), as well as distinctively red colors ($m_{\rm 277W} - m_{\rm 444W} \gtrsim 0.5$). Indeed, the product between the logarithm of the stellar mass and the logarithm of the SFR, $I_{\star}$, nicely isolates DSFGs from other populations, particularly when combined with a red color criterion.

2. We then exploit the COSMOS2025 catalog to search for faint, high-redshift DSFGs through a color-based selection combined with SFR and stellar mass cuts, identifying 18 candidates at $z_{\rm phot} \approx 6$–8. A stacking analysis constrains their mean 1.2 mm flux density to $S_{\rm 1.2mm} = 0.15 \pm 0.02$ mJy, corresponding to a dust-obscured SFR of $\approx 30\,M_{\odot}\,{\rm yr}^{-1}$, assuming standard dust SED templates, and to a typical ${\rm SFR_{IR}/SFR_{total}}$ ratio below or around 0.5. This suggests the presence of a faint population of dusty galaxies within the epoch of reionization, which, together with other confirmed dusty systems in the field, indicates a nonnegligible contribution from dust-obscured star formation to the cosmic history of star formation, even up to $z \sim 7$–8.

3. Using our well-defined surveyed area, we constrained the volume density of these faint high-redshift dusty candidates to be $5.9^{+1.8}_{-1.3} \times 10^{-6}\,{\rm Mpc}^{-3}$, in broad agreement with the massive quiescent systems at $z \approx 3$–5 and the ultra−high-redshift population of bright galaxies at $z > 10$. Finally, we compared the predicted stellar mass growth history of quiescent galaxies with the inferred stellar masses and redshifts of our high-redshift DSFG candidates and with the properties of UV-bright galaxies at $z > 10$ and concluded that the three populations might be evolutionarily linked, with the $z \approx 6$–8 DSFGs being the descendants of the UV-bright $z > 10$ galaxies and the progenitors of the massive $z \sim 3$–5 quiescent galaxies.

While these results suggest the existence of a population of dusty galaxies within the Universe's first billion years—supporting recent findings in the literature—further observations are needed to confirm their redshifts and physical properties, as well as to establish their potential evolutionary connection with other galaxy populations in the early Universe.

Acknowledgments

We thank the anonymous referee for the valuable feedback, which improved the clarity and strengthened the results of this manuscript. We thank Fengwu Sun for sharing their data, which was useful in preparation of Figure 3. We also thanks William Baker for sharing their catalog of quiescent galaxies before publication. D.B.S. gratefully acknowledges support from NSF grant 2407752. M.A. is supported by FONDECYT

grant No. 1252054 and gratefully acknowledges support from ANID Basal Project FB210003 and ANID MILENIO NCN2024_112. G.E.M. acknowledges the Villum Fonden research grants 37440 and 1316. S.F. acknowledges support from the Dunlap Institute, funded through an endowment established by the David Dunlap family and the University of Toronto. Y.F. is supported by JSPS KAKENHI grant Nos. JP22K21349 and JP23K13149. This material is partially based on work supported by the National Science Foundation under award No. 1519126. This Letter makes use of the following ALMA data: ADS/JAO.ALMA#2023.1.00180.L ALMA is a partnership of ESO (representing its member states), NSF (USA) and NINS (Japan), together with NRC (Canada), NSTC and ASIAA (Taiwan), and KASI (Republic of Korea), in cooperation with the Republic of Chile. The Joint ALMA Observatory is operated by ESO, AUI/NRAO and NAOJ. The National Radio Astronomy Observatory and Green Bank Observatory are facilities of the U.S. National Science Foundation operated under cooperative agreement by Associated Universities, Inc.

The JWST data presented in this article were obtained from the Mikulski Archive for Space Telescopes (MAST) at the Space Telescope Science Institute. The specific observations analyzed can be accessed via doi:10.17909/ahg3-e826.

Facilities: ALMA, JWST.

Appendix A
Spectroscopic Confirmation of Three Galaxies

We use observations from the COSMOS-3D program (GO#5893; PI: K. Kakiichi) to search for spectroscopic detections within our final sample of 18 faint DSFG candidates. We use the internal data release processed with the *grizli*[45] reduction pipeline (G. Brammer 2019) in combination with JWST pipeline version 1.18 (see R. A. Meyer et al. 2025 for details). All spectra have been continuum-subtracted.

Figure 5 shows the extracted spectra for three objects with robust line detections, corresponding to spectroscopic redshifts of 7.20, 5.85, and 5.0 (for the latter, conservatively assuming that the single detected is Hα).

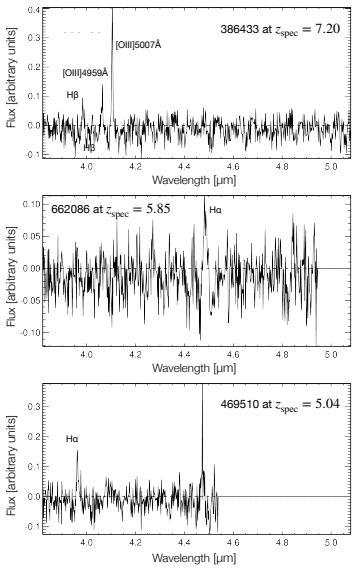

Figure 5. COSMOS-3D spectra of three of our 18 DSFG candidates with detected emission lines. From top to bottom, $ID_{COSMOS2025}$=386433 at $z = 7.20$ (first reported in R. A. Meyer et al. 2025), 662086 at $z = 5.85$ (confirmed by H. B. Akins et al. 2024 using NIRSpec observations), and 469510 at $z = 5.04$, assuming that the line corresponds to Hα (with an artifact at around 4.47 μm).

Appendix B
A Deeper Look into the $I_\star$ Parameter

Here we explore the $I_\star$ parameter in the context of the main sequence (MS) of star-forming galaxies and how a selection based on this quantity relates to a selection based on, for example, offset from the MS (ΔMS). For this purpose, in Figure 6 we plot a representative sample of galaxies within $z \approx 2$–4 (extracted from the COSMOS2025 catalog) along with the MS of star-forming galaxies at $z = 3$ (using the parameterization from J. S. Speagle et al. 2014) and different cuts of $I_\star$ (dotted lines in the figure). A cut in ΔMS would be almost orthogonal to a cut in $I_\star$ and could, in principle, select low-mass galaxies as long as they pass the adopted ΔMS threshold. In contrast, a cut in $I_\star$ would preferentially select massive galaxies on the MS and

[45] https://grizli.readthedocs.io/

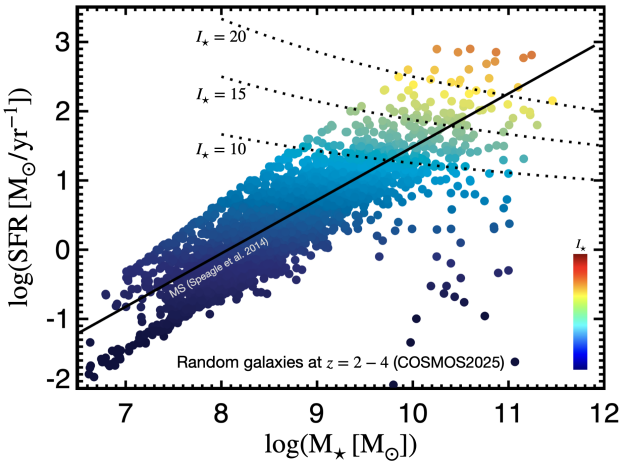

Figure 6. A random subsample of galaxies at $z = 2$–4 from the COSMOS2025 catalog is shown, color-coded by their $I_\star$ values, along with the MS of star-forming galaxies at $z \sim 3$ (J. S. Speagle et al. 2014; solid black line). The dashed lines represent curves of constant $I_\star$ values. As can be seen, a cut at fixed $I_\star$ value allows the selection of starburst galaxies at low stellar masses and MS galaxies at high stellar masses, which can be used to preferentially select DSFGs.

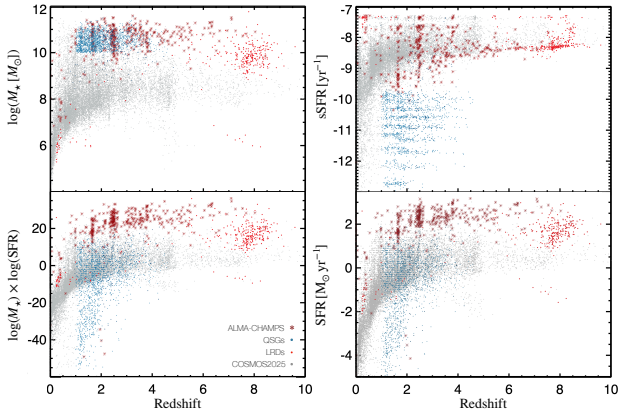

Figure 7. The stellar mass (top left), sSFR (top right), $I_\star$ (bottom left), and SFR (bottom right) as a function of redshift for galaxies in the COSMOS2025 catalog. The gray points represent a random ∼5% subsample of the catalog, while counterparts to other specific subsamples are identified with different colors: red asterisks for the >5σ ALMA CHAMPS galaxies (see Section 2), blue circles for massive quiescent galaxies (W. M. Baker et al. 2026; A. Long 2026, in preparation), and light-red circles for LRDs (H. B. Akins et al. 2024; redundancy intended). As can be seen, the SFR and $I_\star$ are the best parameters to isolate DSFGs from other populations (while the sSFR, for example, works better for separating quiescent galaxies).

would include relatively low mass galaxies only if they are significantly above the MS (i.e., starbursts). Given that some (if not the majority of) DSFGs are known to lie on the high-mass end of the MS and that they could even dominate the high-mass population (e.g., M. J. Michałowski et al. 2012; J. S. Dunlop et al. 2017; A. S. Long et al. 2023; F.-Y. Liu et al. 2026), the proposed selection based on $I_\star$ would result in a higher completeness compared to a selection based on ΔMS, and it would have less contamination compared to selection based on the specific SFR (sSFR).

Appendix C
A Comparison of Different Diagrams to Isolate DSFGs

Most of the DSFGs detected at submillimeter/millimeter wavelengths have been shown to be massive systems, with $M_\star > 10^{10}\,M_\odot$ (e.g., M. J. Michałowski et al. 2012; J. S. Dunlop et al. 2017; U. Dudzevičiūtė et al. 2020; J. McKinney et al. 2025). Despite this, a simple selection criterion based on a stellar mass threshold would suffer from contamination from other kinds of galaxies, particularly at $z \lesssim 3$–4, where massive quiescent galaxies start to rise. This is clearly seen in the top left panel of Figure 7, where we plot different galaxy subsamples. Actually, at $z \lesssim 3$ quiescent galaxies become an increasingly dominant population at these high stellar masses. Similarly, a simple selection based on the sSFR would introduce contamination from low-mass galaxies with lower SFRs than those measured in DSFGs but with comparable—or even higher—sSFR (see middle panel of Figure 7). To alleviate this, other works have implemented selections based on the combination of these two parameters (namely $M_\star$ and sSFR) to preferentially select DSFG candidates (e.g., F.-Y. Liu et al. 2026). Here we explore alternative criteria such as a simple SFR cut and introduce a new parameter, $I_\star$, defined as the product between the logarithm of the stellar mass and the logarithm of the SFR. This parameter seems to perform better in isolating DSFGs, as discussed below.

The bottom left panel of Figure 7 shows $I_\star$ as a function of redshift for the ALMA-selected galaxies and other subsamples. As can be seen, this quantity nicely separates DSFGs from other populations without the necessity of adding extra selection criteria. Although this parameter has no direct physical interpretation, it represents a powerful tool to isolate DSFGs and identify new DSFG candidates. Finally, we note that the SFR performs nearly as well as the $I_\star$ parameter (see bottom right panel of Figure 7). This is thanks to the availability of JWST photometry (including MIRI in some cases), which is less affected by dust attenuation compared to previous catalogs such as COSMOS2020 (J. R. Weaver et al. 2022) that relied primarily on HST data and shorter-wavelength observations. However, $I_\star$ shows slightly higher completeness and lower contamination and is therefore adopted as the preferred method in this manuscript.

ORCID iDs

Jorge A. Zavala https://orcid.org/0000-0002-7051-1100
Andreas L. Faisst https://orcid.org/0000-0002-9382-9832
Manuel Aravena https://orcid.org/0000-0002-6290-3198
Caitlin M. Casey https://orcid.org/0000-0002-0930-6466
Jeyhan S. Kartaltepe https://orcid.org/0000-0001-9187-3605
Felix Martinez, III https://orcid.org/0000-0002-9883-1413
John D. Silverman https://orcid.org/0000-0002-0000-6977
Sune Toft https://orcid.org/0000-0003-3631-7176
Ezequiel Treister https://orcid.org/0000-0001-7568-6412
Hollis B. Akins https://orcid.org/0000-0003-3596-8794
Hiddo Algera https://orcid.org/0000-0002-4205-9567
Karina Barboza https://orcid.org/0000-0003-4660-9762
Andrew J. Battisti https://orcid.org/0000-0003-4569-2285
Gabriel Brammer https://orcid.org/0000-0003-2680-005X
Zheng Cai https://orcid.org/0000-0001-8467-6478
Jaclyn Champagne https://orcid.org/0000-0002-6184-9097
Nicole E. Drakos https://orcid.org/0000-0003-4761-2197
Eiichi Egami https://orcid.org/0000-0003-1344-9475
Xiaohui Fan https://orcid.org/0000-0003-3310-0131
Maximilien Franco https://orcid.org/0000-0002-3560-8599
Yoshinobu Fudamoto https://orcid.org/0000-0001-7440-8832
Seiji Fujimoto https://orcid.org/0000-0001-7201-5066
Steven Gillman https://orcid.org/0000-0001-9885-4589

Ghassem Gozaliasl https://orcid.org/0000-0002-0236-919X
Santosh Harish https://orcid.org/0000-0003-0129-2079
Xiangyu Jin https://orcid.org/0000-0002-5768-738X
Koki Kakiichi https://orcid.org/0000-0001-6874-1321
Darshan Kakkad https://orcid.org/0000-0002-2603-2639
Anton M. Koekemoer https://orcid.org/0000-0002-6610-2048
Ruqiu Lin https://orcid.org/0000-0003-3987-0858
Daizhong Liu https://orcid.org/0000-0001-9773-7479
Arianna S. Long https://orcid.org/0000-0002-7530-8857
Georgios E. Magdis https://orcid.org/0000-0002-4872-2294
Sinclaire Manning https://orcid.org/0000-0003-0415-0121
Crystal L. Martin https://orcid.org/0000-0001-9189-7818
Jed McKinney https://orcid.org/0000-0002-6149-8178
Romain Meyer https://orcid.org/0000-0001-5492-4522
Giulia Rodighiero https://orcid.org/0000-0002-9415-2296
Victoria Salazar https://orcid.org/0000-0001-5331-065X
David B. Sanders https://orcid.org/0000-0002-1233-9998
Marko Shuntov https://orcid.org/0000-0002-7087-0701
Margherita Talia https://orcid.org/0000-0003-4352-2063
Takumi S. Tanaka https://orcid.org/0009-0003-4742-7060
Feige Wang https://orcid.org/0000-0002-7633-431X
Wuji Wang https://orcid.org/0000-0002-7964-6749
Stephen M. Wilkins https://orcid.org/0000-0003-3903-6935
Jinyi Yang https://orcid.org/0000-0001-5287-4242
Min S. Yun https://orcid.org/0000-0001-7095-7543

References

Akins, H. B., Casey, C. M., Champagne, J. B., et al. 2025, arXiv:2508.06607
Akins, H. B., Casey, C. M., Lambrides, E., et al. 2025, The Astrophysical Journal, 991, 37
Algera, H. S. B., Inami, H., Oesch, P. A., et al. 2023, MNRAS, 518, 6142
Arrabal Haro, P., Dickinson, M., Finkelstein, S. L., et al. 2023, Natur, 622, 707
Asada, Y., Willott, C., Muzzin, A., et al. 2026, ApJ, 996, 115
Baker, W. M., Valentino, F., Lagos, C. d. P., et al. 2026, ApJ, 996, 115
Bakx, T. J. L. C., Algera, H. S. B., Jolly, J.-B., et al. 2025, MNRAS,
Barger, A. J., & Cowie, L. L. 2023, ApJ, 956, 95
Bakx, T. J. L. C., Sommovigo, L., Carniani, S., et al. 2021, MNRAS, 508, L58
Barro, G., Pérez-González, P. G., Kocevski, D. D., et al. 2024, ApJ, 963, 128
Barrufet, L., Oesch, P. A., Weibel, A., et al. 2023, MNRAS, 522, 449
Battisti, A. J., da Cunha, E., Jin, S., & Hodge, J. A. 2025, RNAAS, 9, 157
Bing, L., Oliver, S., Xiao, M., et al. 2025, arXiv:2511.08672
Brammer, G., 2019 Grizli: Grism redshift and line analysis software, Astrophysics Source Code Library, ascl:1905.001
Bunker, A. J., Saxena, A., Cameron, A. J., et al. 2023, A&A, 677, A88
Carnall, A. C., Cullen, F., McLure, R. J., et al. 2024, MNRAS, 534, 325
Carnall, A. C., McLure, R. J., Dunlop, J. S., & Davé, R. 2018, MNRAS, 480, 4379
Carniani, S., Hainline, K., D'Eugenio, F., et al. 2024, Natur, 633, 318
Casey, C. M. 2012, MNRAS, 425, 3094
Casey, C. M., Akins, H. B., Shuntov, M., et al. 2024, ApJ, 965, 98
Casey, C. M., Kartaltepe, J. S., Drakos, N. E., et al. 2023, ApJ, 954, 31
Casey, C. M., Narayanan, D., & Cooray, A. 2014, PhR, 541, 45
Castellano, M., Fontana, A., Merlin, E., et al. 2025, A&A, 704, 158
Castellano, M., Fontana, A., Treu, T., et al. 2023, ApJL, 948, L14
Castellano, M., Napolitano, L., Fontana, A., et al. 2024, ApJ, 972, 143
Chen, C.-C., Gao, Z.-K., Hsu, Q.-N., et al. 2022, ApJL, 939, L7
Conroy, C. 2013, ARA&A, 51, 393
Daddi, E., Dannerbauer, H., Krips, M., et al. 2009, ApJL, 695, L176
de Graaff, A., Setton, D. J., Brammer, G., et al. 2025, NatAs, 9, 280
Decarli, R., Walter, F., Venemans, B. P., et al. 2017, Natur, 545, 457
Dickinson, M., Amorin, R., Arrabal Haro, P., et al. 2024, The CANDELS-Area Prism Epoch of Reionization Survey (CAPERS), JWST Proposal. Cycle 3, ID. #6368,
Donnan, C. T., Dickinson, M., Taylor, A. J., et al. 2025, ApJ, 993, 224
Donnan, C. T., McLure, R. J., Dunlop, J. S., et al. 2024, MNRAS, 533, 3222
Driver, S. P., & Robotham, A. S. G. 2010, MNRAS, 407, 2131
Dudzevičiūtė, U., Smail, I., Swinbank, A. M., et al. 2020, MNRAS, 494, 3828
Dunlop, J. S., McLure, R. J., Biggs, A. D., et al. 2017, MNRAS, 466, 861
Endsley, R., Stark, D. P., Lyu, J., et al. 2023, MNRAS, 520, 4609
Finkelstein, S. L., Leung, G. C. K., Bagley, M. B., et al. 2024, ApJL, 969, L2
Franco, M., Akins, H. B., Casey, C. M., et al. 2024, ApJ, 973, 23
Franco, M., Casey, C. M., Koekemoer, A. M., et al. 2025, arXiv:2506.03256
Franco, M., Elbaz, D., Béthermin, M., et al. 2018, A&A, 620, A152
Fudamoto, Y., Oesch, P. A., Schouws, S., et al. 2021, Natur, 597, 489
Fujimoto, S., Kohno, K., Ouchi, M., et al. 2024, ApJS, 275, 36
Fujimoto, S., Oguri, M., Brammer, G., et al. 2021, ApJ, 911, 99
Gehrels, N. 1986, ApJ, 303, 336
Gillman, S., Gullberg, B., Brammer, G., et al. 2023, A&A, 676, A26
Glazebrook, K., Nanayakkara, T., Schreiber, C., et al. 2024, Natur, 628, 277
Greene, J. E., Labbe, I., Goulding, A. D., et al. 2024, ApJ, 964, 39
Harikane, Y., Inoue, A. K., Ellis, R. S., et al. 2025, ApJ, 980, 138
Harish, S., Kartaltepe, J. S., Liu, D., et al. 2025, ApJ, 992, 45
Hashimoto, T., Inoue, A. K., Mawatari, K., et al. 2019, PASJ, 71, 71
Herard-Demanche, T., Bouwens, R. J., Oesch, P. A., et al. 2025, MNRAS, 537, 788
Hodge, J. A., & da Cunha, E. 2020, RSOS, 7, 200556
Hodge, J. A., da Cunha, E., Kendrew, S., et al. 2025, ApJ, 978, 165
Hughes, D. H., Serjeant, S., Dunlop, J., et al. 1998, Natur, 394, 241
Inami, H., Algera, H. S. B., Schouws, S., et al. 2022, MNRAS, 515, 3126
Ito, K., Valentino, F., Brammer, G., et al. 2025, arXiv:2506.22642
Jin, S., Sillassen, N. B., Hodge, J., et al. 2024, A&A, 690, L16
Kakiichi, K., Egami, E., Fan, X., et al. 2024, COSMOS-3D: A Legacy Spectroscopic/Imaging Survey of the Early Universe, JWST Proposal. Cycle 3, ID. #5893,
Kennicutt, R. C., & Evans, N. J. 2012, ARA&A, 50, 531
Labbé, I., van Dokkum, P., Nelson, E., et al. 2023, Natur, 616, 266
Laporte, N., Zitrin, A., Ellis, R. S., et al. 2021, MNRAS, 505, 4838
Liu, D., Lang, P., Magnelli, B., et al. 2019, ApJS, 244, 40
Liu, F.-Y., Dunlop, J. S., McLure, R. J., et al. 2026, MNRAS, 545, staf1961
Long, A. S., Casey, C. M., Lagos, C. d. P., et al. 2023, ApJ, 953, 11
Long, A. S., Casey, C. M., McKinney, J., et al. 2024, arXiv:2408.14546
Manning, S. M., Casey, C. M., Zavala, J. A., et al. 2022, ApJ, 925, 23
Manning, S. M., McKinney, J., Whitaker, K. E., et al. 2025, arXiv:2505.09703
Marrone, D. P., Spilker, J. S., Hayward, C. C., et al. 2018, Natur, 553, 51
Matthee, J., Naidu, R. P., Brammer, G., et al. 2024, ApJ, 963, 129
McKay, S. J., Barger, A. J., Cowie, L. L., & Nicandro Rosenthal, M. J. 2025, ApJ, 988, 135
McKinney, J., Casey, C. M., Long, A. S., et al. 2025, ApJ, 979, 229
Meyer, R. A., Wang, F., Kakiichi, K., et al. 2025, arXiv:2510.11373
Michałowski, M. J., Dunlop, J. S., Cirasuolo, M., et al. 2012, A&A, 541, A85
Mitsuhashi, I., Zavala, J. A., Bakx, T. J. L. C., et al. 2025, arXiv:2501.19384
Naidu, R. P., Oesch, P. A., Brammer, G., et al. 2025, arXiv:2505.11263
Oesch, P. A., Brammer, G., Naidu, R. P., et al. 2023, MNRAS, 525, 2864
Papovich, C., Cole, J. W., Yang, G., et al. 2023, ApJL, 949, L18
Pérez-González, P. G., Barro, G., Annunziatella, M., et al. 2023, ApJ, 946, L16
Rodighiero, G., Bisigello, L., Iani, E., et al. 2023, MNRAS, 518, L19
Schouws, S., Stefanon, M., Bouwens, R., et al. 2022, ApJ, 928, 31
Shuntov, M., Akins, H. B., Paquereau, L., et al. 2025, A&A, 704, 339
Smail, I., Dudzevičiūtė, U., Gurwell, M., et al. 2023, ApJ, 958, 36
Speagle, J. S., Steinhardt, C. L., Capak, P. L., & Silverman, J. D. 2014, ApJS, 214, 15
Sun, F., Yang, J., Wang, F., et al. 2025, arXiv:2506.06418
Taylor, A. J., Kokorev, V., Kocevski, D. D., et al. 2025, ApJL, 989, L7
Umehata, H., Kubo, M., Smail, I., et al. 2026, ApJ, 997, 79
Valentino, F., Brammer, G., Gould, K. M. L., et al. 2023, ApJ, 947, 20
Wang, B., Leja, J., de Graaff, A., et al. 2024, ApJL, 969, L13
Wang, T., Schreiber, C., Elbaz, D., et al. 2019, Natur, 572, 211
Wang, T., Sun, H., Zhou, L., et al. 2025, ApJL, 988, L35
Watson, D., Christensen, L., Knudsen, K. K., et al. 2015, Natur, 519, 327
Weaver, J. R., Kauffmann, O. B., Ilbert, O., et al. 2022, ApJS, 258, 11
Whitaker, K. E., Pope, A., Cybulski, R., et al. 2017, ApJ, 850, 208
Williams, C. C., Alberts, S., Ji, Z., et al. 2024, ApJ, 968, 34
Xiao, M., Oesch, P. A., Elbaz, D., et al. 2024, Natur, 635, 311
Zavala, J. A., Buat, V., Casey, C. M., et al. 2023, ApJL, 943, L9
Zavala, J. A., Casey, C. M., Manning, S. M., et al. 2021, ApJ, 909, 165
Zavala, J. A., Castellano, M., Akins, H. B., et al. 2025, NatAs, 9, 155
Zavala, J. A., Montaña, A., Hughes, D. H., et al. 2018, NatAs, 2, 56